

The Generalized Droop Formula for Low Signal to Noise Ratio Optical Links

Alberto Bononi, *Senior Member, IEEE*, Jean-Christophe Antona, Matteo Lonardi, *Student Member, IEEE*, Alexis Carbo-Méseguer and Paolo Serena, *Member, IEEE*

Abstract—We present a theoretical model that fully supports the recently disclosed generalized droop formula (GDF) for calculating the signal-to-noise ratio (SNR) of constant-output power (COP) amplified coherent links operated at very low SNR. For single-mode nonlinear COP links we compare the GDF-SNR to the better known generalized SNR (GSNR) that uses the Gaussian noise (GN) model for constant-gain (CG) amplifiers. We find that at all medium to large SNRs the GSNR well matches with the GDF, while at GSNR below 6dB the GSNR over-estimates the correct GDF-SNR by more than 0.5dB. Fortunately, the GDF-SNR turns out to be approximately a simple function of the GSNR, which allows adaptation of the widespread GSNR also to very low SNR links. A key finding of this paper is that the end-to-end model underlying the GDF is a concatenation of per-span first-order regular perturbation (RP1) models with end-span power renormalization. This fact allows the GDF to well reproduce the SNR of highly nonlinear systems, well beyond the RP1 limit underlying the GN model. The GDF is successfully extended to the case where the bandwidth/modes of the COP amplifiers are not entirely filled by the transmitted multiplex. Finally, the GDF is extended to CG amplified links and is shown to improve on known GN models of highly nonlinear propagation with CG amplifiers.

Index Terms—Optical amplifiers, Signal Droop, Split-step Fourier method, GN model.

I. INTRODUCTION

Recent improvements in coherent optical systems have enabled an increase of the reach of submarine links beyond 15,000km (see, e.g., [1], [2]) and a decrease of the target signal to noise ratio (SNR) around 7dB in commercial bids [3]. Also, the ongoing evolution towards Spatial Division Multiplexing

(SDM) has paved the way to even lower SNR targets [4], [5]. The submarine systems evolution towards open cables eventually imposes to accurately model the performance of the sole cable, even at low SNR [6]–[8]. Therefore, refining the accuracy of performance prediction models at low SNR has become of great importance, and is the basic motivation for this work.

Amplified spontaneous emission (ASE)-induced signal droop in constant output power (COP) amplifier chains was studied long ago [9]. Today’s submarine systems basically all use COP amplifiers, but most analytical models for single-mode transmission do assume constant-gain (CG) amplifiers, with a few exceptions (e.g., [10]). In the context of SDM submarine transmissions, the term “droop” was introduced a few years ago by Sinkin *et al.* [4], [5], who revived the droop problem in COP amplified SDM links. Antona *et al.* [2], [3] recently proposed a new expression of the received SNR in very-long haul, low-SNR submarine links with coherent detection, which we here call the generalized droop formula (GDF). The formula was originally conceived for linear low-SNR SDM links, and it was next applied also to low-SNR nonlinear single-mode dispersion uncompensated COP-amplified coherent links, where nonlinear interference (NLI) becomes significant. While at standard SNR values the performance of such COP links is well predicted by the generalized SNR (GSNR) [6], [7], [11]–[13] in which NLI variance is usually obtained from the Gaussian Noise (GN) models for CG amplifiers [14]–[19], it was shown in [3] that at very low SNR and for COP amplified links the GDF provides a more accurate SNR prediction. Besides NLI, extensions of the GDF to account for other sources of distributed noise in the transmission fiber were also proposed [2], [3].

This paper (and its conference summary [20]), for the first time provides a full derivation of the GDF introduced in [2], [3], and shows its accuracy against split-step Fourier method (SSFM) simulations in several case studies. The paper compares the GN-calculated GSNR for CG amplifiers against the GDF for two purposes. First, to quantify the SNR values above which the GSNR for CG-amplified links can be safely used for predicting the SNR of COP-amplified

Manuscript received xxxxxxxx xx, xxxx; accepted xxxxxxxx xx, xxxx. Date of publication xxxxxxxx xx, xxxx; date of current version xxxxxxxx xx, xxxx.

A. Bononi, P. Serena, are with the Dipartimento di Ingegneria e Architettura, Università di Parma, Parma 43124, Italy (corresponding author e-mail: alberto.bononi@unipr.it). M. Lonardi was with Università di Parma, and is now with Nokia Bell Labs, Villarceaux, France. J.-C. Antona and A. Carbo-Méseguer are with Alcatel Submarine Networks, Villarceaux, France.

Color versions of one or more of the figures in this paper are available online at <http://ieeexplore.ieee.org>.

Digital Object Identifier xx.xxxx/JLT.xxxx.xxxxxx.

links. Second, the paper derives tight upper and lower bounds to the GDF which are based solely on the GSNR. This means that one may appropriately warp the standard GSNR to get reliable predictions even at the lowest SNRs.

A fair comparison in a low SNR link of the GDF against the GSNR calculated with the most appropriate COP-adapted GN model [10] (which also includes the nonlinear signal-noise interaction normally ignored by standard GN models) will be provided. We will show that the two models yield the same SNR predictions at small to moderate powers, but the GN-based GSNR is optimistic at the largest powers because of its underlying first-order regular perturbation (RP1) assumption [21]: it fails to predict the signal depletion operated by NLI.

The GDF model is instead a concatenation of per-span RP1 models with end-span power renormalization, reminiscent of multi-stage backpropagation [22], [23]. This fact allows the GDF to well reproduce the SNR of highly nonlinear systems, well beyond the RP1 limit underlying the GN models [24]–[26]. Inspired by the GDF, a novel method of assessing when an end-to-end system is well modeled by an RP1 system is presented in the appendix.

The GDF theory is then extended to the more general case where significant out-of-band ASE is present in the system, yielding a new SNR expression that we call the COP-GDF. While working out the extended theory, we found deep connections also with CG amplifier chains with significant nonlinear signal-ASE interactions, for which extensions of the GN theory are known [27], [28]. We here propose a new formula, which we call the CG-GDF. All formulas are checked against accurate SSFM simulations. In particular, COP-GDF and CG-GDF always show the best match with SSFM simulations among known formulas.

The paper is organized as follows. Sections II and III introduce the system model and derive the additive and rearrangement droops. Sec. IV derives the basic GDF, discusses its implications and introduces upper and lower bounds to the GDF. Sec. V presents numerical comparisons of theory against simulations, and GDF against both its approximations and against the GSNR predicted by the extended GN model (EGN) [10], [16]–[19]. Sec. VI extends the GDF to the case when ASE has a larger spectral occupancy than the useful signal. Sec. VII discusses the CG case and derives the new CG-GDF expression. Sec. VIII concludes the paper.

Sections from VI onwards contain new material with respect to that summarized in [20].

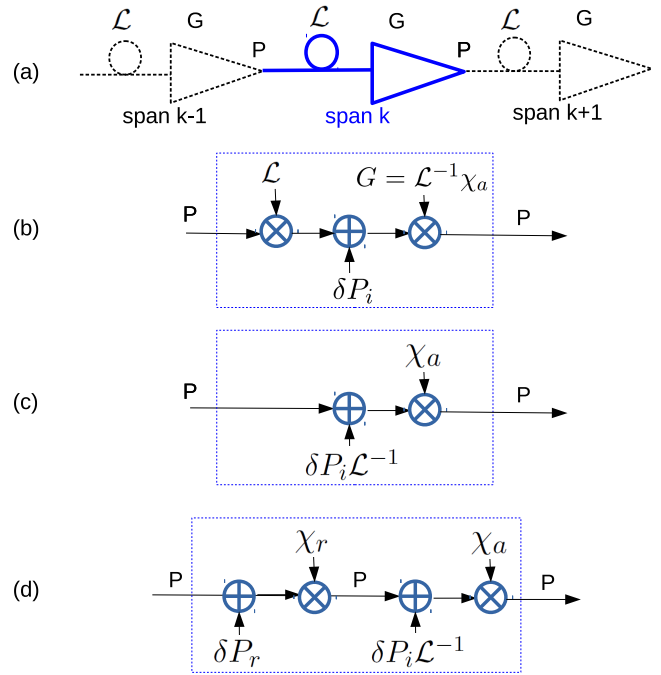


Figure 1. (a) Chain of spans with loss \mathcal{L} with amplifiers with constant output power P and ASE equivalent input power δP_i . Gain must be $G = \mathcal{L}^{-1} \chi_a$ (see text), with $\chi_a < 1$ the ASE-induced power droop. (b) Span power block diagram. (c) Equivalent diagram with loss factored out. (d) Added block diagram also of fiber span with redistribution power δP_r and renormalization to P by a redistribution power droop $\chi_r < 1$.

II. DROOP INDUCED BY POWER ADDITION

Consider the transmission of a mode/wavelength division multiplexed (M/WDM) signal, composed of M spatial modes (each corresponding to two orthogonal polarizations) each composed of an N_c -channel Nyquist-WDM system [29] over a total bandwidth B , along a chain of N identical multi-mode/core fiber (MF) spans. All spans have loss $\mathcal{L} < 1$ and are followed by an end-span amplifier having a total constant output power (COP) equal to P . We assume the multiplex total launched power is P , and that loss \mathcal{L} and amplifier gain G are the same at all wavelengths and modes. We also assume the amplifier has a filter that suppresses all out-of band/mode ASE noise, so that ASE and signal spectra are flat over the same bandwidth B . The Nyquist-WDM assumption and the assumption that ASE and signal exist on the same spectral range will be relaxed in Section VI.

As seen in Fig. 1(a), the chain has at each span k a total input power P , and a total output power P . Hence in the ideal case of noiseless amplifiers, the amplifier gain $G = \mathcal{L}^{-1}$ exactly compensates the loss. The span block diagram for real amplifiers is shown in Fig. 1(b), where an equivalent input ASE noise power $\delta P_i = Mh\nu FB$ (where h is Planck's constant, ν is the multiplex center frequency, F is the noise figure

[30], B the amplification bandwidth and M is the number of modes) is injected in the amplifier, hence the gain $G = \mathcal{L}^{-1}\chi_a$ must decrease by a *droop* factor $\chi_a < 1$ from the ideal case to “squeeze” the transiting signal and make room for the local ASE noise in the output power budget P . By shifting back the term \mathcal{L}^{-1} upstream of the addition block (i.e., by “factoring out” the loss) the block of Fig. 1(b) is seen to be equivalent to that in Fig. 1(c), from which we read the span input-output power budget as: $(P + \delta P_i \mathcal{L}^{-1})\chi_a = P$, and thus deduce the droop

$$\chi_a = \left(1 + \frac{\delta P_i \mathcal{L}^{-1}}{P}\right)^{-1} \triangleq (1 + SNR_{a1}^{-1})^{-1} \quad (1)$$

where $\delta P_i \mathcal{L}^{-1}$ is the output ASE that would be generated by an end-span amplifier with gain \mathcal{L}^{-1} , and we implicitly defined SNR degraded at the single amplifier as

$$SNR_{a1} \triangleq \frac{P}{\delta P_i \mathcal{L}^{-1}}. \quad (2)$$

The droop is in fact the total power gain (in fact, a loss) of each amplified span, so that the desired multiplex signal power at the output of the N -th amplifier is

$$P_s(N) = P \prod_{k=1}^N \mathcal{L}G = P\chi_a^N \quad (3)$$

which tells us that the desired signal becomes weaker along the nominally transparent line because of the accumulation of ASE which reduces the amplifier gain G because of the COP constraint. The accumulated ASE at the output of the N -span chain (over all modes and amplified WDM bandwidth B) is thus

$$P_a(N) = P - P_s(N) = P(1 - \chi_a^N). \quad (4)$$

By equating (3),(4) we find that signal and ASE powers become equal at $N \cong \ln 2 \cdot SNR_{a1}$.

Note that the above analysis remains unchanged if the amplifiers are noiseless, but an external lumped crosstalk (e.g., power leaking from a competing optical multiplex of power P crossing an optical multiplexer/demultiplexer together with our multiplex of interest at an optical node before the final optical amplification, or, e.g., transmitter impairments at the booster amplifier) of power $\delta P_i = \alpha_{ex}P$ is injected in its place, where α_{ex} is the external crosstalk coefficient. In presence of both ASE and external crosstalk the droop χ_a in (1), that we more generally call the *addition droop*, uses an added power $\delta P_i = Mh\nu FB + \alpha_{ex}P$, where uncorrelation between the two noise sources is assumed when summing power.

III. DROOP INDUCED BY POWER REDISTRIBUTION

The transmission fiber is indeed not ideal and operates a power redistribution during propagation because of several physical mechanisms. Let’s for the moment concentrate on one of these, namely, the nonlinear Kerr effect. Focus on Fig. 1(c) where the fiber loss has been factored out. We now apply a first-order regular perturbation approximation of the Kerr distortion generated within span k , called nonlinear interference (NLI), as in the GN and similar perturbative models [12], [13], [15]. We then impose that the power in/out of the fiber be conserved. Thus, we get a power-flow diagram of the fiber+amplifier block as depicted in Fig. 1(d), where now the power redistribution during propagation appears as a new input sub-block in which a perturbation $\delta P_r = \alpha_{NL}P^3$ is added to the input signal P (α_{NL} is the per-span NLI coefficient [31]), and then a *redistribution droop* χ_r forces the perturbed signal back to power P , namely, $(P + \delta P_r)\chi_r = P$. This yields

$$\chi_r = \left(1 + \frac{\delta P_r}{P}\right)^{-1} \triangleq (1 + SNR_{r1}^{-1})^{-1} \quad (5)$$

where we implicitly defined the SNR degraded at the single amplifier by the redistribution mechanism as

$$SNR_{r1} \triangleq \frac{P}{\delta P_r} = \frac{1}{\alpha_{NL}P^2} \quad (6)$$

where the second equality holds specifically for the NLI redistribution mechanism¹.

In other terms, we first apply a per-span RP1 perturbation, and then re-normalize signal plus perturbation power at fiber end, thus reducing at each span the power-divergence problem intrinsic in the RP1 approximation [21]. Other redistribution mechanisms for which the above theory applies verbatim are:

1) the thermally-induced guided-acoustic wave Brillouin scattering (GAWBS) [32], for which $\delta P_r = \gamma_{GAWBS}\ell P$, where γ_{GAWBS} [km⁻¹] is the GAWBS coefficient, and ℓ [km] is the span length;

2) the inter-mode/core linear crosstalk in the MF, for which $\delta P_r = \gamma_X\ell P$, where γ_X [km⁻¹] is the crosstalk coefficient [33].

Thus including all three (uncorrelated) effects, we have in (5),(6): $\delta P_r = \alpha_{NL}P^3 + (\gamma_{GAWBS} + \gamma_X)\ell P$.

IV. SIGNAL TO NOISE RATIO

According to the proposed per-span power-flow diagram in Fig. 1(d), the total span power gain seen by

¹The model in [20] swaps the addition and multiplication operations in the power rearrangement sub-block in Fig. 1(d), which yields $P\chi_r + \delta P_r = P$ leading to $\chi_r = 1 - \delta P_r/P$, whose numerical value in practice coincides with the expression in (5). Eq. (5), however, leads exactly to the GDF (7).

the transiting signal, i.e., the overall span droop, is the product of addition and redistribution droops: $\chi \triangleq \chi_r \chi_a$. By the same reasoning as in (3),(4), if the launch power is P , then the desired multiplex signal power at the output of the N -th amplifier is $P_s(N) = P\chi^N$ and therefore by the constant output power constraint the accumulated *addition+redistribution noise* at the output of the N -span chain (over all modes and amplified WDM bandwidth B) is $P_a(N) + P_r(N) = P(1 - \chi^N)$.

Hence the optical SNR (OSNR) at the output of the chain from amplifiers 1 to N , i.e., the ratio of total multiplex signal power to total noise power at the output of the N -th amplifier, using (1),(5) is obtained as,

$$OSNR = \frac{1}{\left[(1 + SNR_{a1}^{-1})(1 + SNR_{r1}^{-1})\right]^N - 1} \quad (7)$$

which is the generalized droop formula (GDF) presented for the first time in [2], [3]. Please note a key assumption of the GDF model: the power additions expressed by the power block diagram, Fig. 1, tacitly imply that the noise sources injected at each span are uncorrelated from all others, and thus, in particular, assuming an incoherent accumulation of NLI.

The GDF can be re-arranged into the key formula [2], [3]

$$1 + \frac{1}{OSNR} = \left[\left(1 + \frac{1}{SNR_{a1}}\right) \left(1 + \frac{1}{SNR_{r1}}\right) \right]^N \quad (8)$$

which we call the *product rule for inverse droop*. It hints at the generalization [2], [3]

$$1 + \frac{1}{OSNR} = \prod_{k=1}^N \left(1 + \frac{1}{SNR_{a1k}}\right) \left(1 + \frac{1}{SNR_{r1k}}\right) \quad (9)$$

for an inhomogeneous chain, where SNR_{a1k} is the local ASE-reduced OSNR at amplifier k , and similarly SNR_{r1k} for redistribution noise. We prove this generalization in Appendix A.

We conclude this section with a key observation. When the dominant part of the power spectral density (PSD) of each of the above impairments remains flat as the input signal PSD, then the per-tributary signal to noise ratio SNR for this flat-loss, flat-gain system will remain equal to $OSNR$, since both signal and noises get filtered over the same tributary bandwidth and mode. Hence from now on, we will drop the ‘‘O’’ in the OSNR, and treat P and B as the launched input power and bandwidth of each tributary. In section VI we will generalize the per-tributary SNR expression to the case where ASE occupies a larger bandwidth/number of modes than the signal multiplex.

SNR approximations

We derive here upper and lower bounds to the GDF. Define

$$SNR_1 \triangleq (SNR_{a1}^{-1} + SNR_{r1}^{-1})^{-1} \quad (10)$$

as the SNR degraded by the total noise generated at a single span. Let $x \triangleq SNR_1^{-1}$, which is normally a very small term. Then, as proposed in [3], the GDF denominator can be bounded as: $\chi^{-N} - 1 \geq (1+x)^N - 1 \geq Nx(1 + \frac{1}{2}(N-1)x)$ by expanding to 2nd order in Taylor. Thus an upper-bound to the GDF is

$$SNR \leq \frac{SNR_s}{1 + \frac{1}{2}(1 - \frac{1}{N})(SNR_s)^{-1}} \quad (11)$$

where

$$SNR_s \triangleq \frac{1}{Nx} \equiv \frac{SNR_1}{N} \quad (12)$$

is the SNR we would calculate with the standard noise accumulation formula for CG amplifiers. We call it the standard SNR.

Now let $y = \frac{1}{2}(1 - \frac{1}{N})Nx \geq 0$. Since $(1+y)^{-1} \geq 1-y$, then we can lower-bound the upper-bound (11) and luckily get a lower bound to the GDF-SNR as well:

$$SNR \geq \frac{1 - \frac{1}{2}(1 - \frac{1}{N})Nx}{Nx} = SNR_s - \frac{1}{2}(1 - \frac{1}{N}). \quad (13)$$

To understand the scope of the above approximations, Fig. 2(a) shows in black solid line a plot of the GDF-SNR²:

$$SNR \cong ((1 + SNR_1^{-1})^N - 1)^{-1} \quad (14)$$

versus the standard $SNR_s \equiv SNR_1/N$. The figure also shows its upper-bound (UB) eq. (11) and lower-bound (LB) eq. (13) (both dash-dotted), and the SNR_s itself (dotted). Fig. 2(b) shows the same as (a), but with the SNR axis expressed in dB. The curves in Fig. 2 were obtained for $N = 100$, but they remain essentially unchanged for any $N \gtrsim 40$.

We observe in Fig. 2(a) and can prove analytically that: i) the LB (13) crosses zero at $SNR_s = \frac{N-1}{2N}$ and becomes negative (not physically acceptable) below that; ii) the gap from SNR_s to GDF (and to all its approximations) converges for increasing SNR_s to the asymptotic value $\frac{1}{2}(1 - \frac{1}{N})$, and the gap from SNR_s to GDF exceeds 90% of its asymptotic value at $SNR_s > 1.66$ (2.2dB) for any N . The constant gap in linear units translates into a variable gap when SNR is in dB, i.e., to a small dB-gap at large SNR_s and a large dB-gap at lower SNR_s . The dB plot also does not clearly show the $\sim 1/2$ asymptotic linear gap.

²Since SNR_{a1}^{-1} and SNR_{r1}^{-1} are normally very small, then the product $SNR_{a1}^{-1}SNR_{r1}^{-1}$ is a higher-order negligible term. Hence the GDF (7) and expression (14) are practically identical.

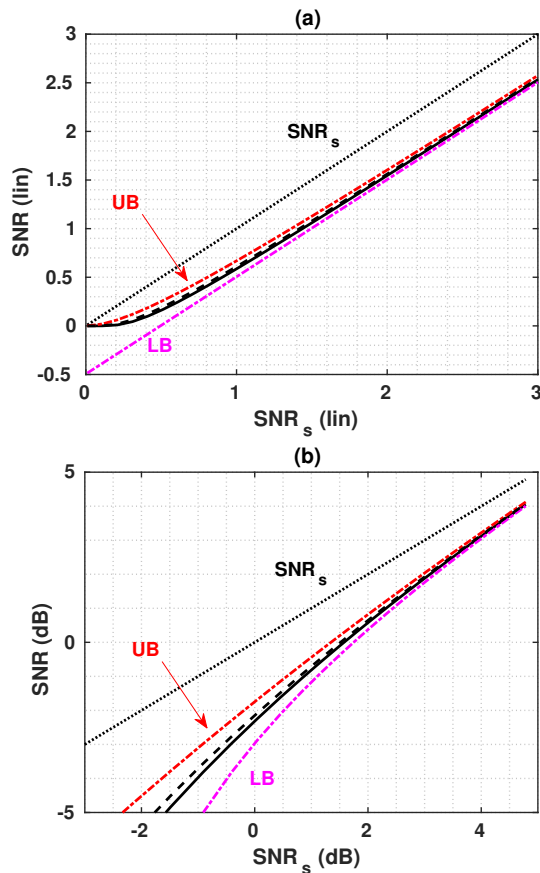


Figure 2. (a) Black solid: GDF (14) versus the standard SNR: $SNR_s = SNR_1/N$. Dash-dot: Upper-bound (UB, red) eq. (11) and Lower-Bound (LB, magenta) eq. (13). Black dotted: SNR_s . Black dashed: approximation (15). (b) Corresponding figure when SNRs are in dB. Curves obtained for $N = 100$, but they remain essentially unchanged for any $N \geq 40$.

These observations will be useful when interpreting the numerical SNR results in Section V.

Our best approximation to the GDF (which also turns out to be a tighter upper-bound) is shown in dashed line in Fig. 2, and can be obtained by taking $10 \log_{10}(\cdot)$ of each side of eq. (11) and then linearizing the logarithm. The resulting expression in dB is:

$$SNR(dB) \geq SNR_s(dB) - \frac{e^{dB} \cdot \frac{1}{2} \left(1 - \frac{1}{N}\right)}{SNR_s} \quad (15)$$

where SNR_s without (dB) indicates its linear value, $e^{dB} \triangleq 10 \log_{10}(e) \cong 4.34$, and e is Neper's number.

To make the physical meaning of the above approximations to the GDF explicit, let's focus on the case of single-mode fibers ($M = 1$), with ASE and NLI only. Define

$$\beta \triangleq h\nu FB\mathcal{L}^{-1} \quad (16)$$

as the ASE power (per mode) generated at the output of each amplifier of gain \mathcal{L}^{-1} over the per-tributary receiver bandwidth B . Then from (10),(2),(6) we get

$$SNR_s \equiv \frac{1}{N \left(\frac{\beta}{P} + \alpha_{NL} P^2 \right)} \quad (17)$$

where in (2) we used $\delta P_i \mathcal{L}^{-1} = \beta$, and the α_{NL} term is, per Fig. 1(d), the single-span NLI coefficient computed over the same per-tributary bandwidth B as β . We recognize the standard SNR (17) to be the widely used GSNR for dispersion-uncompensated systems with coherent detection in which the end-to-end NLI coefficient $N\alpha_{NL}$ is routinely obtained by the GN models for CG amplified links, the most precise of which is the EGN model [16]–[19] that accounts for the details of the modulation format. We thus observe from Fig. 2(a) that the GSNR for CG amplified links can also be safely used for predicting the SNR of COP-amplified links, at all SNR values for which its over-estimation by 1/2 in linear units is tolerable. The good news is that even at the smallest SNRs, where the GDF is more accurate for COP amplified links, the newly obtained GDF upper and lower bounds are based solely on the value of the GSNR, which means we may appropriately warp the standard GSNR to get reliable predictions even at the smallest SNRs.

The above discussion should have convinced the reader that, although using the GN-calculated GSNR (for CG amplified links) for comparison with the GDF (for COP amplified links) is definitely unfair, yet the comparison has a didactic purpose in the light of Fig. 2, since from the GSNR we can derive good approximations to the GDF. A fair comparison of the GDF with the COP-adapted EGN model in [10] will be provided and discussed later on in the numerical results section.

Finally, we note that although the above GDF model assumes uncorrelated NLI span by span, in numerical computations we can approximately account for the NLI span-by-span correlations by first calculating the NLI coefficient of the entire link (e.g., using the CG EGN model) and then dividing by N , so that now the α_{NL} to be used in the GDF is a span-averaged coefficient and, for RP1 end-to-end links at large SNR (where COP and CG amplifications are equivalent), the GDF predicts the same correct SNR as that of the EGN model. Appendix B provides a more in depth discussion on this topic.

V. NUMERICAL CHECKS

We present here three single-mode dispersion-uncompensated case studies with quasi Nyquist-WDM signals where we verify the above formulas against SSFM simulations (unless otherwise stated, the simulation step size was selected to keep a nonlinear phase per step of $3 \cdot 10^{-3}$ rad):

case A is the 228x78km polarization-division multiplexed (PDM) quadrature phase-shift keying (QPSK) WDM link analyzed in [3]. The propagation fiber was an EX2000TM (loss 0.169 dB/km, fiber nonlinear

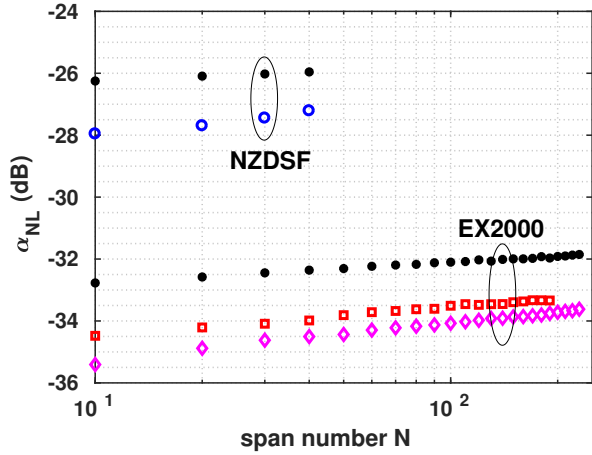


Figure 3. Values in dB of span-averaged NLI coefficient α_{NL} (mW^{-2}) versus spans N , used in theoretical formulas for the 3 case studies (diamonds for case A, squares for case B, circles for case C). Also, filled circles show values for Gaussian modulation.

coefficient $n_2 = 2.5 \cdot 10^{-20} \text{ m}^2/\text{W}$, effective area $110 \mu\text{m}^2$, dispersion 20.7 ps/nm/km). Optical amplifiers had a noise figure F of 8dB. The number of channels was 16, with channel spacing 37.5 GHz and symbol rate 34.17 Gbaud. SSFM simulations were carried out with a simulated bandwidth 60 times the symbol rate, and ASE was removed outside the WDM bandwidth. The number of transmitted symbols was 64800. This case is representative of a modern ultra-long submarine link (see, e.g., [1]).

case B) is the 190x78km PDM 16-quadrature amplitude modulation (16QAM) link analyzed in [3]. All data are the same as in case A, except for the number of spans (now 190) and the modulation format. The number of transmitted symbols was 2^{16} . This case was selected as it gives a comparably low SNR to case A and is useful to test the accuracy of the GDF with a different modulation format, although a 16QAM format is not efficient at the low SNRs we find.

case C) is the 40x120km PDM-QPSK link analyzed in [10, Fig. 3]. The propagation fiber was a non-zero dispersion shifted fiber (NZDSF) (loss 0.22 dB/km, fiber NL coefficient $n_2 = 2.6 \cdot 10^{-20} \text{ m}^2/\text{W}$, effective area $70.26 \mu\text{m}^2$, dispersion 3.8 ps/nm/km). Noise figure F was 5dB. The number of channels was 15, with channel spacing 50 GHz and symbol rate 49 Gbaud. Again the simulated bandwidth was 60 times the symbol rate, and ASE was removed outside the WDM bandwidth. The number of transmitted symbols was 2^{13} . This case was selected since it allows a fair comparison of the GDF against the most accurate available EGN model for COP amplified links [10].

We accounted just for ASE and NLI, and the GDF

formula explicitly is

$$SNR = \frac{1}{\left[\left(1 + \frac{\beta}{P}\right) (1 + \alpha_{NL} P^2) \right]^N - 1} \quad (18)$$

For all 3 cases, we will present results at the stated number of spans, as well as some results at lower span numbers, all multiples of 10. Fig. 3 shows the values of the span-averaged α_{NL} we have used in the theoretical formulas in the 3 cases (diamonds for case A, squares for case B, circles for case C), along with the values for Gaussian modulation (filled circles). We note in passing that an α_{NL} that grows with N is an indication of self-nonlinearity becoming more important than cross-nonlinearity as N increases, which is typical of small WDM systems [31].

We begin by presenting in Fig. 4 the received SNR versus transmitted power per channel P for all 3 cases at their maximum distance. In all 3 sub-figures we report: the GSNR (17) (dashed black) and the GDF (18) (solid blue), along with their linear and nonlinear asymptotes (dotted); the SSFM simulations at constant output power (symbols: diamonds for case A, squares for case B, circles for case C); the upper and lower bounds UB (11), LB (13) (both dash-dotted), and the approximation (15) (dashed). Values of span-averaged α_{NL} estimated from the CG EGN model and used in theoretical formulas were: $\alpha_{NL} = [4.34, 4.63, 19.01] \times 10^{-4} \text{ (mW}^{-2}\text{)}$ for cases A,B,C, respectively. These can be read from Fig. 3.

We first note in all cases the very good fit of the GDF with SSFM simulations. As explained in Appendix B, although the GDF assumes uncorrelated noises at each span, our use of the span-averaged NLI coefficient α_{NL} allows us to have good fit also in links where span-by-span correlations are significant, as in our 3 selected cases where Fig. 3 shows a marked variation of the span-averaged α_{NL} with span number N .

Next note that the GDF at these low SNRs is always below the GSNR and its asymptotes have a different slope than those of the GSNR. As already noted in Fig. 2, this is an artifact of the dB representation of the SNR, since the SNR gap between the two curves is about 1/2 (in linear units) for GSNR above ~ 1.66 (2.2 dB).

Finally, we note that UB and LB and approximation (15) are basically coinciding with the GDF in cases A and B on the shown scale, and they become visible only in the tails of the SNR “bell-curve” in case C. The gap to UB, LB and (15) is quite small, as already appreciated in Fig. 2. In particular, approximation (15) is the best among all, and is basically coinciding with the GDF over most of the shown ranges.

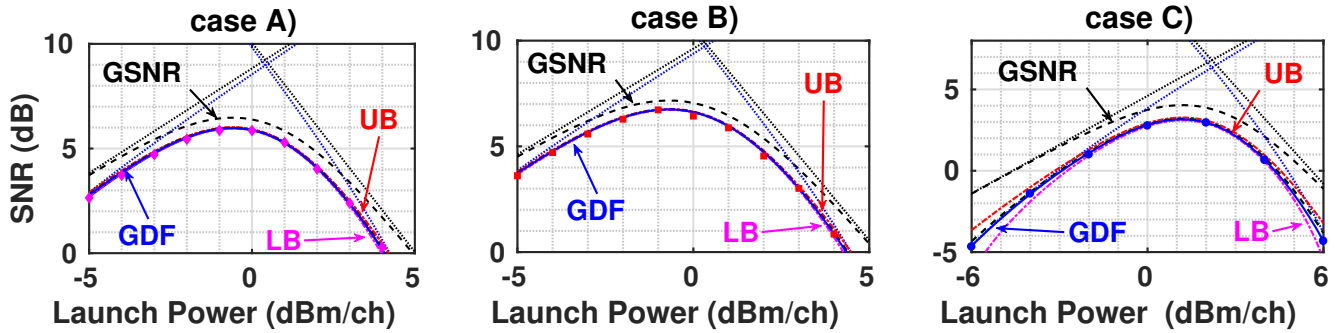


Figure 4. SNR(dB) versus power per channel P (dBm) for: **case A)** 228x78km EX2000 uncompensated link, 34.17 Gbd PDM-QPSK, 16-channel @ 37.5GHz spacing [3]; **case B)** 190x78km EX2000 uncompensated link, 34.17 Gbd PDM-16QAM, 16-channel @ 37.5GHz [3]; **case C)** 40x120km NZDSF uncompensated link, 49-Gbd PDM-QPSK, 15-channel @ 50GHz [10]. In each plot: Symbols: SSFM simulations. Blue solid: GDF eq. (18). Black dashed: GSNR eq. (17). Linear and nonlinear asymptotes also shown in dotted lines. GDF approximations: Red dash-dotted: upper-bound (UB) (11); Magenta dash-dotted: lower-bound (LB) (13); black dashed: approximation (15).

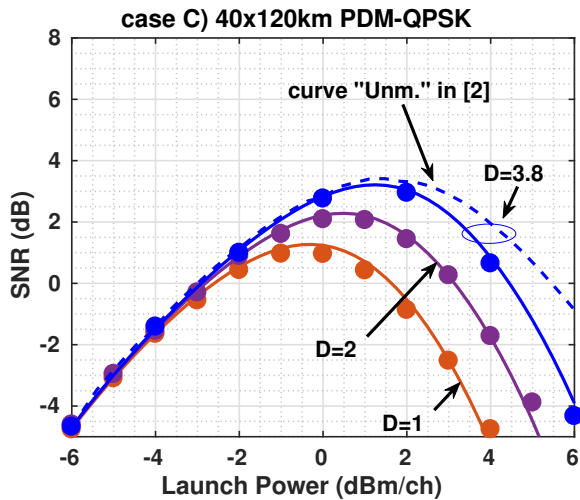


Figure 5. Case C) SNR versus launch power when lowering fiber dispersion D from 3.8 down to 1 ps/nm/km. Symbols: simulations. Solid: GDF. Dashed blue line is SNR predicted by the COP-EGN model in [10, Fig. 5, label “Unm.”].

Fig. 5 concentrates on the SNR versus power in case C and has a twofold purpose. First, it shows not only the GDF, in blue solid line (same curve as in Fig. 4 along with the corresponding SSFM simulations (circles)) but also the predictions of the COP-EGN model in [10] (dashed blue, Cfr. [10, Fig. 5, label “Unm.”]). This figure reports a fair comparison of GDF with the most appropriate EGN model for this link. It is seen that the low to mid-power portion of the SNR well matches with the GDF, but then the RP1-based EGN model becomes optimistic at the largest powers, where the local-RP1 power-renormalized concatenation implicit in the GDF is instead able to well reproduce the SNR even in deep “signal depletion” by NLI (more discussion about the RP1 limits is provided in Appendix B).

The second purpose of Fig. 4 is to show the re-

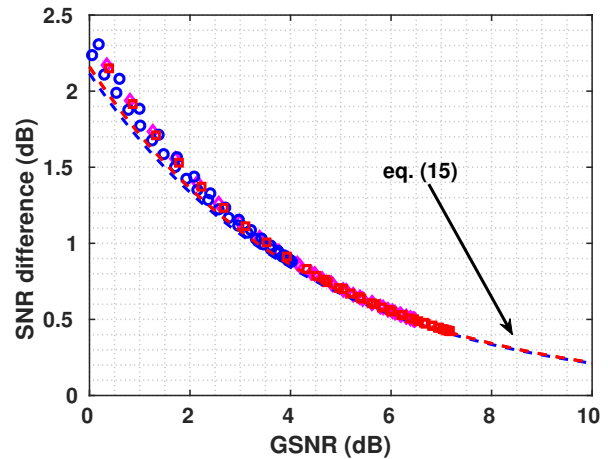


Figure 6. Gap $GSNR(dB) - SNR_{GDF}(dB)$ versus $GSNR(dB)$. Symbols (diamonds for case A, squares case B, circles for case C): exact gap, as visible in Fig. 4. Dashed: approximation (15).

silience of the GDF at lower dispersions. We show the SNR versus power of the system in case C when the NZDSF fiber dispersion is artificially lowered to 2 and 1 ps/nm/km. We see that the GDF-SNR well reproduces the simulated SNR over the whole power range at all considered dispersions.

A. Comparisons with the GSNR

Since the GSNR is the reference formula for nonlinear propagation with coherent detection, it is important to quantify its gap in performance to the GDF for COP-amplified links.

SNR gap: We here discuss the gap from $GSNR$ eq. (17) to SNR_{GDF} eq. (18). The bounds we have found all hint at a 1-1 relation between the two SNRs. This is not exactly so, but almost. Fig. 6 plots the gap $GSNR(dB) - SNR_{GDF}(dB)$ versus $GSNR(dB)$.

Symbols for the three cases (diamonds for case A, squares for case B and circles for case C) indicate the exact gap between the theoretical SNRs (we measure the gap from Fig. 4 in each case scanning from low to high power, and report the values in Fig. 6), while the dashed lines indicate the gap as expressed by the best approximation (15). Especially for case C (circles) it is evident that the SNR_{GDF} is not a 1-1 function of $GSNR$, but to a good extent we may well approximate the gap for all systems by eq. (15). The gap does not exceed 2.5dB for $GSNR$ down to 0 dB.

Optimal power at max SNR: The optimal power P_o at maximum SNR is obtained in the GN model [12] by setting the derivative of $GSNR$ w.r.t. P to zero, yielding the condition $\beta = 2\alpha_{NL}P_o^3$ (i.e., ASE is twice the NLI at P_o) and the explicit optimal GN power $P_{oGN} = (\beta/2/\alpha_{NL})^{1/3}$.

Similarly, the GDF-SNR is maximum at the power P_o that makes the total droop $\chi(P_o)$ closest to 1, leading to the condition $\beta = \frac{2}{\chi(P_o)}\alpha_{NL}P_o^3$, i.e., ASE is *slightly more than twice* the NLI at P_o . This leads to $P_o = P_{oGN}\chi^{1/3} \lesssim P_{oGN}$, since the droop per span $\chi = \chi_a\chi_r$ is always practically very close to 1. Thus the optimal P_o for the GDF is in practice the same as in the GN case,

Spectral efficiency per mode: A lower-bound on the capacity per mode of the nonlinear optical channel for dual-polarization transmissions is obtained from the equivalent additive white Gaussian noise (AWGN) Shannon channel capacity, i.e., by considering the NLI as an additive white Gaussian process independent of the signal. Hence a lower-bound on spectral efficiency per mode is [5], [6], [15]: $SE = 2\log_2(1 + SNR)$ [b/s/Hz]. Its top value SE_o is achieved at P_o using its corresponding top SNR.

For fixed distance, symbol rate, and noise figure, the GDF-SNR and the GSNR just depend on the NLI per-span parameter α_{NL} . The span-averaged α_{NL} values for the AWGN capacity-achieving Gaussian modulation are reported with filled circles in Fig. 3 for both the EX2000 and the NZDSF links.

Fig. 7(a) reports (a lower-bound to) the top SE_o versus span number N when using in the spectral efficiency formula either the GSNR (dashed curve, SE_{GN}) and GDF-SNR (filled circles, SE_{GDF}) obtained for the EX2000 and the NZDSF links with Gaussian modulation. The figure shows that a noticeable departure of the correct SE_{GDF} from the SE_{GN} occurs only at SE_{GN} values below 5 b/s/Hz.

It is simple to prove that the SE gap from GN to GDF $\Delta SE \triangleq SE_{GN} - SE_{GDF}$ is well approximated at large N and at all powers (not only at top) by

$$\Delta SE \cong \frac{2}{\ln(2)} \frac{GSNR}{1 + 2GSNR + 2GSNR^2} \quad (19)$$

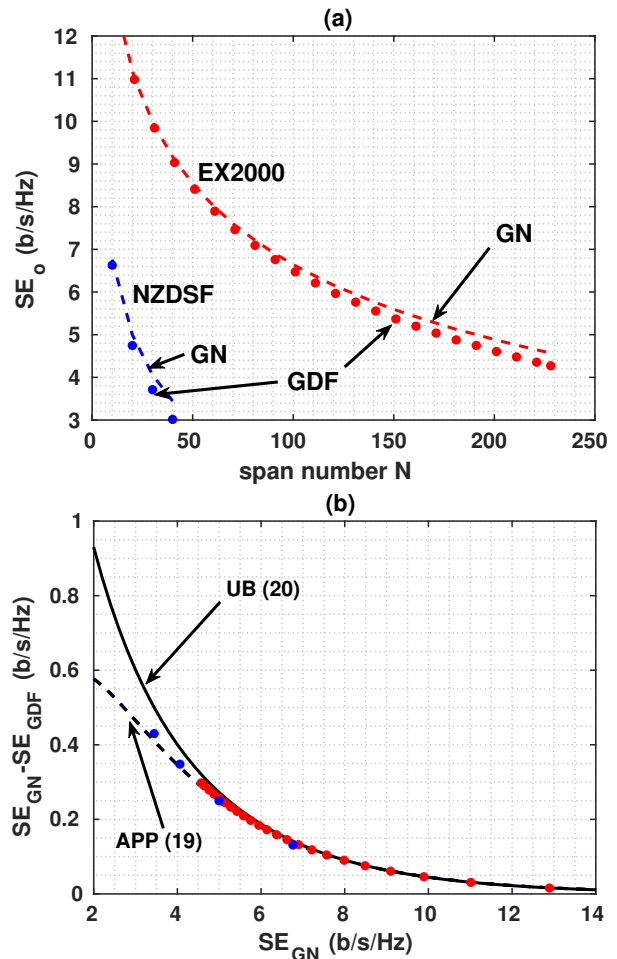


Figure 7. (a) (lower-bound to) top spectral efficiency SE_o (b/s/Hz) versus span number N , obtained for the EX2000 (case A/B) and the NZDSF (case C) links with Gaussian modulation. Dashed: SE_{GN} that uses the GSNR. Filled circles: SE_{GDF} that uses the GDF-SNR. (b) Filled circles: gap $SE_{GN} - SE_{GDF}$ versus SE_{GN} . Solid: UB (20). Dashed: approximation (19).

and upper bounded by

$$\Delta SE \leq \frac{1}{\ln(2)(GSNR + 1/2)} \quad (20)$$

which are plotted in Fig. 7(b) versus SE_{GN} in dashed and solid line, respectively, together with the exact gap (filled circles). Curve (19) can be taken as a good approximation to all shown cases. From the figure, it is seen that using the standard GSNR we over-estimate SE by less than 0.35 [b/s/Hz] at SE_{GN} above 4 [b/s/Hz], and over-estimate SE by between 0.6 and 0.9 [b/s/Hz] at $SE_{GN} = 2$ [b/s/Hz].

VI. LIMITS OF THE GDF

Unfortunately, when the amplified modes M_a and amplified bandwidth B_a exceed the signal modes M and signal occupied bandwidth $B = N_c B_{rx}$ (possible gaps between WDM channels are not counted), the

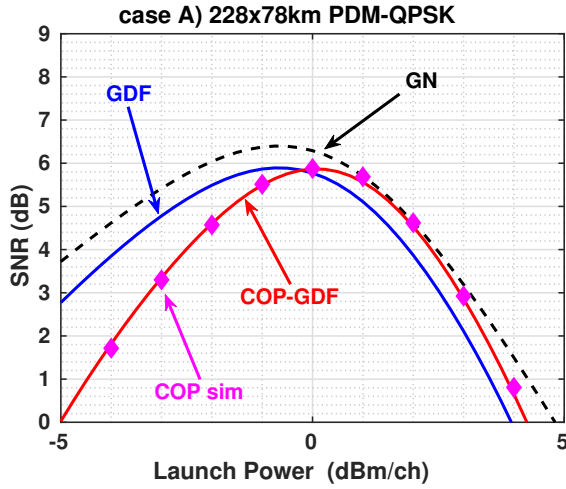


Figure 8. Case A) SNR versus launch power when amplifier bandwidth is $B_a = 60B_{rx}$, $B_{rx} = 34.17$ GHz, and ASE unfiltered. 16 PDM-QPSK channels, spacing $\Delta f = 37.5$ GHz. Symbols: simulations with COP saturation power $16P_t$. We show: the GSNR (17) and the raw GDF (18) (where $B \rightarrow B_{rx}$ and $P \rightarrow P_t$); and the COP-GDF, eqs. (23), (26).

GDF ceases to be accurate, and the *amplifier fill-in efficiency*:

$$\eta_A \triangleq \frac{MN_c}{M_a N_a} \quad (21)$$

with $N_a \triangleq B_a/B_{rx}$, plays a major role in setting performance.

As a numerical example, we consider the 228x78km 16-channel single-mode ($M = M_a = 1$) PDM-QPSK case study A, but now ASE is present over the whole amplified (and simulated) bandwidth $B_a = 60B_{rx}$, with $B_{rx} = 34.17$ GHz. In this system we have $\eta_A = 0.266$. This small number should be checked against the value $\eta_A = 0.91$ for case A in Fig. 4, where ASE is filtered over the WDM bandwidth and the basic GDF very well matches simulations.

Fig. 8 shows the per-tributary SNR versus launch power per tributary P_t (saturation power is in general $P = MN_c P_t$). Symbols are SSFM simulations. We also see in solid line the GSNR (17) and the raw GDF (18) (where in the referenced equations we set $B \rightarrow B_{rx}$ and $P \rightarrow P_t$). We note that with a low η_A the GDF ceases to well match the simulations. This is mostly due to the fact that, because of the relevant out-of-band ASE, the actual ASE-droop is larger and the actual NLI-droop is smaller than what the GDF predicts. The next sub-section explains the tricks necessary to modify the basic GDF to cope with such a scenario.

A. The COP-GDF

Let $P_s(N)$, $P_a(N)$, $P_r(N)$ be the total cumulated signal, ASE and NLI redistribution power from the link

input up to the output of span N . Assuming equal per-tributary powers, at the per-tributary receiver the SNR is:

$$\begin{aligned} SNR &= \left(\frac{P_s(N)}{MN_c} \right) / \left(\frac{P_a(N)}{M_a N_a} + \frac{P_r(N)}{MN_c} \right) \\ &= \frac{P_s(N)}{P_a(N)\eta_A + P_r(N)} \end{aligned} \quad (22)$$

where we assumed that NLI is the same at all tributaries and exists only over the same modes/spectral range as the signal multiplex. It is evident from (22) that SNR evaluation, differently from the basic GDF (7), now requires a separate evaluation of both $P_a(N)$ and $P_r(N)$. These can be calculated explicitly as shown in (36) in Appendix A, yielding

$$SNR = \frac{\prod_{m=1}^N \chi_m}{\sum_{k=1}^N [(\chi_a^{-1} - 1)\chi_{rk}^{-1}\eta_A + \chi_{rk}^{-1} - 1] \prod_{m=k}^N \chi_m} \quad (23)$$

which requires an explicit evaluation of the ASE droop χ_a (30) and of the redistribution droop χ_{rk} (32).

Specifically, regarding $\chi_a = (1 + SNR_{a1}^{-1})^{-1}$, this is span-independent, since $\delta P_i = M_a N_a h\nu F B_{rx}$, so that

$$\begin{aligned} SNR_{a1} &\triangleq \frac{P}{\delta P_i \mathcal{L}^{-1}} = \frac{MN_c P_t}{M_a N_a h\nu F B_{rx} \mathcal{L}^{-1}} \\ &= \eta_A P_t / \beta \end{aligned} \quad (24)$$

where we used definition of β (eq.(16) where $B \rightarrow B_{rx}$), and the definition of η_A (21).

Regarding the NLI droop $\chi_{rk} = (1 + SNR_{r1k}^{-1})^{-1}$ in eq. (32), this is now span-dependent because, due to the COP constraint, the out-of-band/mode ASE (O-ASE) reduces the *effective* tributary power P_e that generates NLI, more and more as the spans increase.

To find the correct per-tributary effective power $P_e(k)$ generating NLI at span k we reason as follows. At each span $k = 1, \dots, N$, the total power that effectively contributes to the NLI generation is not $P = MN_c P_t$, but P minus the O-ASE power entering span k , $P_{ASE,O}(k)$, which we now calculate.

The locally generated output O-ASE at each amplifier is $\beta' = \beta N_a (M_a - M) + \beta (N_a - N_c) M$, i.e., the sum of the whole ASE over non-signal modes and the out-of-band ASE on signal modes. With our definitions, this simplifies to $\beta' = \beta \left(\frac{1}{\eta_A} - 1 \right) MN_c$. Hence the cumulated (and drooped) O-ASE up to span k is

$$P_{ASE,O}(k) \triangleq \beta' (\chi_2 \cdots \chi_{k-1} + \chi_3 \cdots \chi_{k-1} + \dots + \chi_{k-1} + 1)$$

where the final 1 is due to the O-ASE generated at amplifier $k-1$ which is not drooped. By approximating each droop as just the ASE droop: $\chi_j \cong \chi_a$ we

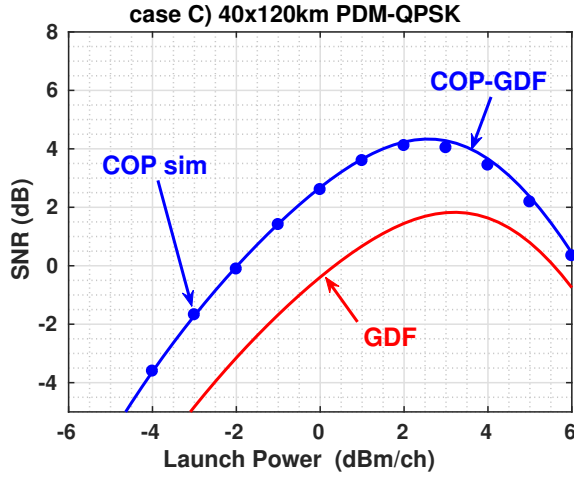


Figure 9. Case C) SNR versus launch power P_t , Cfr. Fig. 4 (15-channel 49Gb PDM-QPSK 40x120km NZDSF link with $\eta_A = 0.98$). ASE filtered on WDM bandwidth, but now channel spacing has doubled to $\Delta f = 100$ GHz, yielding an amplifier fill-in efficiency $\eta_A = 0.49$. Symbols: simulations with COP saturation power $15P_t$. We show: the basic GDF (18) where $B \rightarrow B_{rx} = 49GHz$ and $P \rightarrow P_t$, and the COP-GDF, eq. (23),(26).

thus finally get the effective power and the single-span nonlinear SNR as

$$\begin{cases} P_e(k) = \frac{P - P_{ASE,O}(k)}{MN_c} \cong P_t - \beta \left(\frac{1}{\eta_A} - 1 \right) \frac{1 - \chi_a^{k-1}}{1 - \chi_a} \\ SNR_{r1k} = \frac{P}{\delta P_{rk}} \equiv \frac{P_t}{\alpha_{NL} P_e(k)^3} \end{cases} \quad (25)$$

In summary, the resulting improved SNR formula, which we call the *COP-GDF*, is calculated by eq. (23), where using (24) and (25) we have

$$\begin{cases} \chi_a^{-1} = 1 + \beta / (\eta_A P_t) \\ \chi_{rk}^{-1} \cong 1 + \alpha_{NL} P_t^2 \left(1 - \frac{\beta}{P_t} \left(\frac{1}{\eta_A} - 1 \right) \frac{1 - \chi_a^{k-1}}{1 - \chi_a} \right)^3 \end{cases} \quad (26)$$

For case study A, Fig. 8 also reports the COP-GDF and shows that it well matches simulations. Similar results are obtained for case B and are not reported.

We show in Fig. 9 for case study C what happens when channel spacing is doubled to 100 GHz with respect to Fig. 4, and thus the amplifier fill-in efficiency is halved to $\eta_A = 0.49$. We see that the basic GDF formula badly fails, but the COP-GDF well matches the SSFM simulations.

VII. THE CONSTANT-GAIN CASE

For CG amplifiers, the extension of the GN model to include the nonlinear signal-noise interaction, and its induced signal power depletion, was tackled in [28] with a rigorous end-to-end RP1 model (which inspired the COP-amplifier end-to-end RP1 model in [10]), and heuristically in [27]. While the RP1 model in [28] has the same intrinsic inability as the model in [10] to

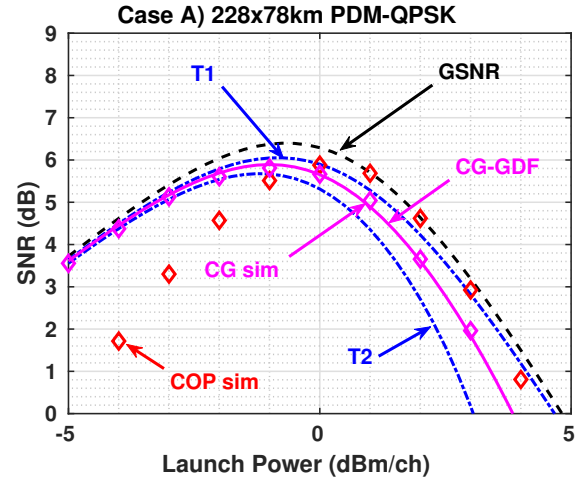


Figure 10. Case A) SNR versus launch power P_t when amplifier bandwidth is $B_a = 60\Delta f$, $\Delta f = 37.5$ GHz, and ASE unfiltered, as in Fig. 8. Symbols: simulations for both CG and COP. We show: the GSNR (black dash); the T1 and T2 formulas, eq. (27),(28) (blue dash-dot); and the CG-GDF, eq. (23),(29) (purple, solid).

cope with the NLI-induced droop at large power, the heuristic models in [27] do go beyond the RP1 limits. We next review such models, and introduce our new contribution, namely the CG-GDF, that uses the Turin's group physical intuitions [27] to extend the COP-GDF ideas and yield a very accurate SNR estimation formula even for the CG case.

The CG-SNR formulas in [27] are the following:

T1 formula: it calculates $SNR = \frac{P_t}{N\beta + P_{NLI}}$ with

$$P_{NLI} = \alpha_{NL} \sum_{n=0}^{N-1} (P_t + n\beta)^3 \quad (27)$$

that approximately accounts for ASE-signal nonlinear interaction by suitably modifying the estimated NLI variance [27, eq. (5)]³. Note that this formula assumes that the ASE useful for nonlinear calculations is the one over the signal bandwidth, since O-ASE is ineffective for CG amplifiers.

T2 formula: it calculates

$$SNR = \frac{P_t - P_{NLI}}{N\beta + P_{NLI}} \quad (28)$$

as first proposed in [34], with P_{NLI} as in (27).

For case study A), Fig. 10 reports the tributary SNR versus launch power P_t for both CG and COP amplifiers, when amplifier bandwidth is $B_a = 60B_{rx}$ and ASE is unfiltered, same as in Fig. 8. Symbols are the simulations for both CG and COP amplifiers, the dashed curve is the GSNR, the dash-dotted curves are the T1 and T2 formulas eq. (27), (28), and the

³Summation in [27] runs 1 to N , but in our simulations the launched power is without ASE, hence we sum 0 to $N - 1$.

solid curve is the new CG-GDF formula that we will describe below.

Regarding SSFM simulations, we first note a shift of the CG SNR with respect to the COP SNR, much in line with the results in [3, Fig 2(b)]. The low-power SNR of the CG case is larger than the COP case because it does not experience ASE-induced droop; the high-power SNR of the CG case is smaller than the COP case because of the span-by-span increase of power in CG that generates nonlinearity.

Regarding the T-formulas (T1, T2), we note that T1 overestimates the simulated CG SNR, while T2 with depletion under-estimates the CG SNR. All the CG curves (simulations, T-formulas, CG-GDF) at low powers tend to coincide with the theoretical GSNR curve, as they should.

A. The CG-GDF

The trouble with the T-formulas is that they try to model a strongly nonlinear system with an amended end-to-end RP1 system. The amendments, however, do contain the correct physical intuition. So the key to the new CG-GDF is to use the intuition [27] about the effective power for NLI generation, eq. (27), but with a re-normalized RP1 per-span model instead of the end-to-end RP1 GN model.

In CG mode we can consider only the ASE and NLI on the per-tributary bandwidth (O-ASE does not affect the SNR). The power-flow diagram is again given by Fig. 1(d), where now we have $\chi_a = 1$, i.e., no ASE droop, and $\delta P_i \mathcal{L}^{-1} \equiv \beta$. As in (27), we now let $\delta P_{rk} = \alpha_{NL}(P_t + (k-1)\beta)^3$.

The new SNR formula, which we call the *CG-GDF*, is thus calculated by eq. (23), where we now use $\chi_k = \chi_{rk}$, $\eta_A = 1$, and replace

$$\begin{cases} (\chi_a^{-1} - 1) \rightarrow \beta/P_t \\ \chi_{rk}^{-1} \rightarrow 1 + \alpha_{NL}P_t^2(1 + (k-1)\frac{\beta}{P_t})^3. \end{cases} \quad (29)$$

In the example of case A), Fig. 10 shows an excellent match between CG-simulations and the CG-GDF. A similarly good match is obtained in the remaining cases B and C.

VIII. CONCLUSIONS

In this paper, we presented a new analytical model to fully theoretically support the GDF disclosed by Antona *et al.* in [2], [3], which includes various fiber power-redistribution mechanisms such as Kerr nonlinearity, GAWBS, and internal and external crosstalk. We verified the GDF against simulations in three published case studies drawn from [3], [10].

We provided upper and lower bounds to the GDF. Using the tightest upper-bound we provided analytical

expressions of the SNR gap from the GSNR to the GDF-SNR, and the corresponding Shannon spectral efficiency (SE) gap. We showed that the gaps can be effectively expressed only in terms of the GSNR and its corresponding SE, SE_{GN} . We showed that the SE gap (per mode) is bounded between 0.6 and 0.9 b/s/Hz when SE_{GN} is as low as 2 b/s/Hz, and it decreases as SE_{GN} increases, e.g., it is less than 0.2 b/s/Hz when the SE_{GN} is above 6 b/s/Hz.

We extended the GDF to the case where ASE has larger bandwidth/mode occupancy than the signal. The resulting COP-GDF equation depends only on the amplifier fill-in efficiency η_A , eq. (21), and was found to very well match simulations in all considered cases. Finally, we extended the GDF theory to include constant-gain amplifier chains, and we derived the new CG-GDF SNR expression that matches simulations better than any other previously known formula.

One of the key theoretical results is that the end-to-end model underlying all GDF expressions is a concatenation of per-span RP1 models with end-span power renormalization. This fact allows the GDFs to well reproduce the SNR of highly nonlinear systems even at very low SNR, well beyond the RP1 limit underlying the GN model based on which the GSNR is calculated. Appendix B provides a novel analytical method (inspired by the GDF) of monitoring when a given transmission line ceases to be well modeled by an RP1 system.

APPENDIX A: GDF FOR INHOMOGENEOUS SPANS

The generalization of the GDF model to the inhomogeneous case goes as follows. The k -th span now has input power P_{k-1} , fiber span loss $\mathcal{L}_k < 1$ and an end-span amplifier operated in COP mode with fixed output power P_k , $k = 0, \dots, N$ (where P_0 is the launched power) and a gain G_k which, in absence of ASE-induced droop, would be $G_k = P_k/(P_{k-1}\mathcal{L}_k)$. With ASE droop the gain is smaller by a factor $\chi_{ak} < 1$. The power flow diagram for the inhomogeneous case is similar to the homogenous case of Fig. 1, where i) all quantities are span- k dependent; ii) the multiplicative output factor in diagrams (c), (d) is now $\chi_{ak}P_k/P_{k-1}$ instead of only χ_a ; iii) in diagram (d) the input sub-block has input/output power P_{k-1} , while the output sub-block has P_{k-1} in and P_k out.

From the modified diagram (d) we thus derive:

1) the power balance at the output sub-block: $(P_{k-1} + \delta P_{ik}\mathcal{L}_k^{-1})\chi_{ak}\frac{P_k}{P_{k-1}} = P_k$, which yields

$$\chi_{ak} = \left(1 + \frac{\delta P_{ik}\mathcal{L}_k^{-1}}{P_{k-1}}\right)^{-1} \triangleq (1 + SNR_{a1k}^{-1})^{-1} \quad (30)$$

where we implicitly defined the SNR degraded by ASE at the single amplifier as

$$SNR_{a1k} \triangleq \frac{P_{k-1}}{\delta P_{ik} \mathcal{L}_k^{-1}}. \quad (31)$$

2) the power balance at the input sub-block: $(P_{k-1} + \delta P_{rk})\chi_{rk} = P_{k-1}$, which yields

$$\chi_{rk} = \left(1 + \frac{\delta P_{rk}}{P_{k-1}}\right)^{-1} \triangleq (1 + SNR_{r1k}^{-1})^{-1} \quad (32)$$

where we implicitly defined the SNR degraded by power redistribution at the single amplifier as

$$SNR_{r1k} \triangleq \frac{P_{k-1}}{\delta P_{rk}}. \quad (33)$$

Define the span total droop as the product of addition and redistribution droops: $\chi_k \triangleq \chi_{rk}\chi_{ak}$. The power block diagram of the k -th span in (modified) diagram (d) shows that the total span power-gain seen by the transiting signal is $(P_k/P_{k-1})\chi_k$, hence the desired multiplex signal power at the output of the N -th amplifier is

$$P_s(N) = P_0 \prod_{k=1}^N (P_k/P_{k-1})\chi_k = P_N \prod_{k=1}^N \chi_k$$

so that the total noise power after N spans is $P_a(N) + P_r(N) = P_N(1 - \prod_{k=1}^N \chi_k)$.

Hence the OSNR at the output of the chain from amplifiers 1 to N , i.e., the ratio of total multiplex signal power to total noise power at the output of the N -th amplifier, is obtained as

$$OSNR = \frac{1}{\left[\prod_{k=1}^N \left(1 + \frac{1}{SNR_{a1k}}\right) \left(1 + \frac{1}{SNR_{r1k}}\right)\right] - 1} \quad (34)$$

which leads to the general product rule for inverse droops, eq. (9) in the main text.

For the calculation of the per-tributary SNR it is necessary instead to have the individual expression of $P_a(N)$, $P_r(N)$, as seen in eq. (22) in the main text. It is possible to read off the modified diagram (d) the update rule for useful signal, additive and redistribution noise at any span k as:

$$\begin{aligned} P_s(k) &= P_s(k-1)\chi_k(P_k/P_{k-1}) \\ P_a(k) &= (P_a(k-1) + \delta P_{ik} \mathcal{L}_k^{-1} \chi_{rk}^{-1})\chi_k(P_k/P_{k-1}) \\ P_r(k) &= (P_r(k-1) + \delta P_{rk})\chi_k(P_k/P_{k-1}) \end{aligned} \quad (35)$$

with initial conditions: $P_s(0) = P_0$, $P_a(0) = P_r(0) = 0$. The second and third recursions are of the kind: $u(k) = (u(k-1) + b_k)a_k$, whose general solution when $u(0) = 0$ is: $u(N) = \sum_{k=1}^N b_k \prod_{m=k}^N a_m$.

Hence, using $\delta P_{ik} \mathcal{L}_k^{-1} \equiv P_{k-1}(\chi_{ak}^{-1} - 1)$ and $\delta P_{rk} \equiv P_{k-1}(\chi_{rk}^{-1} - 1)$ from (30),(32), the formal solutions are

$$\begin{aligned} P_s(N) &= P_N \prod_{m=1}^N \chi_m \\ P_a(N) &= P_N \sum_{k=1}^N (\chi_{ak}^{-1} - 1) \chi_{rk}^{-1} \prod_{m=k}^N \chi_m \\ P_r(N) &= P_N \sum_{k=1}^N (\chi_{rk}^{-1} - 1) \prod_{m=k}^N \chi_m \end{aligned} \quad (36)$$

Although this closed-form solution is pleasing, the recursion (35) is the one we use for calculations.

APPENDIX B: ON THE SPAN-AVERAGED NLI COEFFICIENT

In this appendix we discuss the use in the GDF of the span-averaged NLI coefficient in place of the single-span coefficient α_{NL} , as a trick to approximately include NLI span-by-span correlations that would otherwise be completely neglected by the intrinsically incoherent GDF model i.e., the block diagram in Fig. 1d.

Consider a homogeneous link composed of N identical spans. When power P and number of spans N are ‘‘sufficiently small’’ (and this statement will be made precise in section B.2 of this appendix), the end-to-end link is well described by an RP1 model, and the end-to-end NLI coefficient $a_{NL}(N)$ can be analytically calculated by, e.g., the EGN formula [16]–[19]. Such a coefficient is not merely N times the single-span coefficient α_{NL} (again possibly calculated by the EGN), because of span correlations. The span-averaged NLI coefficient is defined as $\bar{\alpha}_{NL} \triangleq a_{NL}(N)/N$ and is larger than α_{NL} .

Consider now the GDF model. Each span is modeled as an RP1 system with end-span power renormalization. When the end-to-end link behaves as an RP1 system and the SNR is large enough (such that COP and CG amplifications are equivalent), using the span average NLI coefficient in the GDF (i.e., in the NLI perturbation $\delta P_r = \bar{\alpha}_{NL} P^3$ used to define the nonlinear droop χ_r) gives the same correct SNR as that predicted by the EGN model. This is the main reason for choosing $\bar{\alpha}_{NL}$ in place of α_{NL} in the GDF.

We divide the rest of this appendix into two parts. The first shows how the ‘‘incoherent’’ GDF (i.e., using α_{NL}) performs compared to the ‘‘coherent’’ GDF that uses $\bar{\alpha}_{NL}$ as in the main text (in the main text we used the same symbol α_{NL} also for the span-averaged value). The second discusses when power P and number of spans N can be considered ‘‘sufficiently small’’ for the end-to-end link to behave as an RP1 system, which sets a limit to the validity of the RP1 assumption.

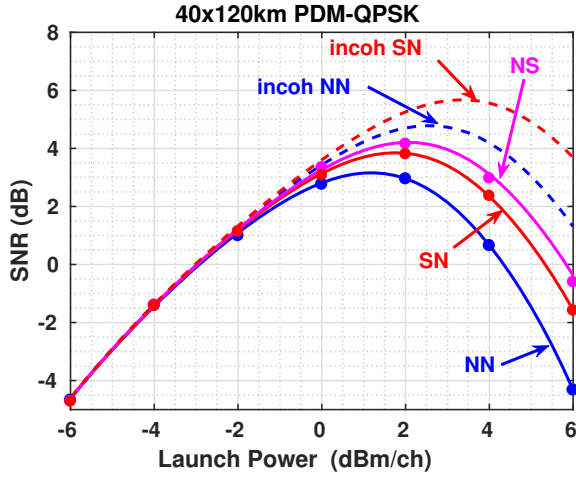


Figure 11. SNR versus power P for the 40x120km PDM-QPSK system (Cfr. case C in main text) for: (solid blue, label NN): homogeneous NZDSF line using span-averaged NLI coefficient in GDF (same curve as in Fig. 5); (dashed blue, label “Incoh NN”): same as previous but using the single-span NLI coefficient in GDF; (red solid, label “SN”) line with 20 SMF spans + 20 NZDSF spans, using span-averaged NLI coefficient in GDF; (dashed red, label “Incoh SN”): same as previous but using the single-span NLI coefficients for NZDSF and SMF in GDF; (purple solid, label “NS”) line with 20 NZDSF spans + 20 SMF spans, using span-averaged NLI coefficient in GDF. Circles with corresponding colors denote checks by SSFM simulations.

B1. “Incoherent” vs “Coherent” GDF

We first concentrate on homogeneous links, i.e., those with identical spans. For the 40-NZDSF-span line with 15 PDM-QPSK channels at 49 Gbaud and 50 GHz spacing of case C in the main text, Fig. 11 shows in blue solid line the SNR calculated with the GDF using the span-averaged NLI coefficient, same curve as in Fig. 4 and Fig. 5 in main text. The corresponding “incoherent” GDF using the single-span NLI coefficient is shown in blue dashed line in Fig. 11 (label “Incoh NN”). We note how off the “incoherent” GDF predictions are, and thus how effective the trick of using the span-averaged coefficient is. Similar results are obtained in the homogeneous links of cases A and B in Fig. 4, but not reported.

Next we consider how the trick of using the span-averaged NLI coefficient in the GDF works for inhomogeneous links. As a variation of case C, we considered various arrangements of the 40 spans where the fiber type for each span could be either NZDSF or single-mode fiber (SMF) with loss 0.22 dB/km, fiber NL coefficient $n_2 = 2.5 \cdot 10^{-20} \text{ m}^2/\text{W}$, effective area $80 \mu\text{m}^2$, dispersion 17 ps/nm/km. We present the case of 20 SMF spans followed by 20 NZDSF spans (label “SN”) and the opposite arrangement “NS”, where we found the largest discrepancy of the “coherent GDF” with simulations. For both the SN and NS cases the number of SSFM symbols was

increased to 25600. Solid red and magenta curves in Fig. 11 show the corresponding GDF curves with span-averaged NLI coefficient ($\bar{\alpha}_{NL} = 1.03 \cdot 10^{-3} \text{ mW}^{-2}$ for NS and $\bar{\alpha}_{NL} = 1.28 \cdot 10^{-3} \text{ mW}^{-2}$ for SN), which even in this worst case show a reasonable match with their corresponding SSFM simulations (circles). The largest discrepancy with simulations is in the NS case, and is 0.2dB at most. The dashed red curve shows instead the “incoherent” GDF for both SN and NS cases, given by $SNR = \left(\left[\left(1 + \frac{\beta}{P} \right) (1 + \alpha_{NL,N} P^2)^{1/2} (1 + \alpha_{NL,S} P^2)^{1/2} \right]^N - 1 \right)^{-1}$, with $\alpha_{NL,N} = 7.29 \cdot 10^{-4}$ and $\alpha_{NL,S} = 1.25 \cdot 10^{-4} \text{ mW}^{-2}$ the single-span NLI coefficients for NZDSF and SMF, respectively. As seen, again such “incoherent” GDF is far off the corresponding SSFM simulations.

In conclusion, the trick of the span-average NLI coefficient makes the GDF work well in homogeneous links and in some inhomogeneous links, although more investigation about inhomogeneous links is necessary.

B2. Monitoring the end-to-end RP1 assumption

How small should the power and the number of spans be for the RP1 assumption to hold?

The end-to-end NLI coefficient a_{NL} obtained by the EGN formula can be verified by split-step Fourier method (SSFM) simulations when ASE is absent (note that without ASE, COP amplifiers behave exactly as CG amplifiers). The theoretical SNR at the end of the link should be according to the EGN model

$$SNR = \frac{1}{a_{NL} P^2}. \quad (37)$$

The estimated \hat{a}_{NL} is routinely obtained from the samples of the received constellation scatter diagram.

We ran SSFM simulations of the homogeneous PDM-QPSK system in [3], case A. Fig. 12 shows with stars the estimated span-averaged NLI coefficient⁴ $\bar{\alpha}_{NL}(P)$, i.e., \hat{a}_{NL}/N , plotted versus P for various span numbers N . We note that the estimated $\bar{\alpha}_{NL}(P)$ sharply increases with power P , while according to the RP1 theory it should be power independent. Indeed, its asymptotic low power value does coincide with the $\bar{\alpha}_{NL}$ value obtained analytically from the EGN model. However, a marked difference of the estimated $\bar{\alpha}_{NL}(P)$ from the low-power value is a symptom of the failure of the RP1 assumption: higher-order perturbations are setting in.

⁴Please note the use of boldface, to distinguish $\alpha_{NL}(P)$ which is P dependent, from the span-average coefficient α_{NL} which is power independent.

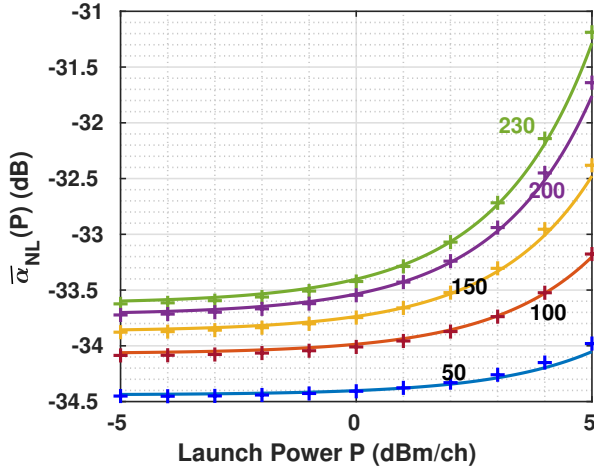


Figure 12. dB-value of span-averaged power-dependent NLI coefficient $\bar{\alpha}_{NL}(P)$ [mW^{-2}] in eq. (39) versus launch power P (thick solid) and its estimate from SSFM simulated scatter diagrams in absence of ASE (crosses). SSFM step-size with nonlinear phase $5 \cdot 10^{-4}$ (rad). EGN values of span-average NLI coefficient used in (39): $\bar{\alpha}_{NL} = [-34.44, -34.07, -33.87, -33.72, -33.62]$ (dB) for $N = [50, 100, 150, 200, 230]$ spans.

The analytical solid curves in Fig. 12, which well match simulations, plot instead an analytical formula for the power-dependent span-averaged coefficient which we derive below, based on the GDF model (which, as stated, goes beyond the end-to-end RP1 range of validity).

According to the NLI-only GDF, the received SNR is

$$SNR = \frac{P\chi_r^N}{P(1 - \chi_r^N)} \triangleq \frac{1}{N\bar{\alpha}_{NL}(P)P^2} \quad (38)$$

with $\chi_r = (1 + \bar{\alpha}_{NL}P^2)^{-1}$, and we force it to be equal to an EGN-like SNR using a power-dependent span-averaged NLI coefficient, whose explicit expression thus is

$$\bar{\alpha}_{NL}(P) = \frac{(1 + \bar{\alpha}_{NL}P^2)^N - 1}{NP^2} \quad (39)$$

and is our novel analytical formula for the power-dependent span-averaged coefficient. We may use it to specify the range of validity of the RP1 assumption, as follows.

While the ‘‘RP1’’ SNR (37) plotted versus P is a straight line with slope -2 in a dB-dB scale, the GDF (38) forecasts without ASE a more than linear decrease. We may declare the largest power P^* below which the RP1 assumption holds to be that power at which $\bar{\alpha}_{NL}(P^*) = 1.1\bar{\alpha}_{NL}$ (using, e.g., a 10% increase from RP1 value). Such a power approximately is $P^* \cong \sqrt{\frac{0.2}{(N-1)\bar{\alpha}_{NL}}}$. So the RP1 assumption well holds if $(N - 1)P^2 \lesssim 0.2/\bar{\alpha}_{NL}$ and the bound just depends on the theoretical span-averaged coefficient

$\bar{\alpha}_{NL}$. As a numerical example, refer to the 40-span homogeneous case C shown in Fig. 5, where the SNR predicted by both GDF and the RP1 COP-EGN model in [10] are shown in blue lines. The span-average coefficient was $\bar{\alpha}_{NL} = 1.83e - 3$, so that $P^* \cong 2.24$ dBm, which is where roughly the COP-EGN curve significantly departs from the more correct GDF, exactly because of the failure of the end-to-end RP1 assumption.

REFERENCES

- [1] J. Cai *et al.*, ‘‘51.5 Tb/s Capacity over 17,107 km in C+L Bandwidth Using Single-Mode Fibers and Nonlinearity Compensation,’’ *J. Lightwave Technol.*, vol. 36, no. 11, pp. 2135-2141, 2018
- [2] J.-C. Antona *et al.*, ‘‘Performance of open cable: from modeling to wide scale experimental assessment,’’ in *Proc. SubOptic*, New Orleans (LA), 2019, paper OP 7-2.
- [3] J.-C. Antona, A. Carbo Méséguer, and V. Letellier, ‘‘Transmission Systems with Constant Output Power Amplifiers at Low SNR Values: a Generalized Droop Model,’’ in *Proc. Opt. Fiber Commun. (OFC)*, San Diego (CA), 2019, paper M1J.6.
- [4] O. V. Sinkin *et al.*, ‘‘Maximum Optical Power Efficiency in SDM-Based Optical Communication Systems,’’ *Photon. Technol. Lett.*, vol. 29, no. 13, pp. 1075-1077, Jul. 2018.
- [5] O. V. Sinkin *et al.*, ‘‘SDM for Power-Efficient Undersea Transmission,’’ *J. Lightw. Technol.*, vol. 36, no. 2, pp. 361-371, Jan. 2018.
- [6] V. Kamalov *et al.*, ‘‘The subsea fiber as a Shannon channel,’’ in *Proc. SubOptic*, New Orleans (LA), 2019, paper OP12-2.
- [7] E. Rivera Hartling *et al.*, ‘‘Subsea Open Cables: A Practical Perspective on the Guidelines and Gotchas,’’ in *Proc. SubOptic*, New Orleans (LA), 2019. Available at <https://suboptic2019.com/download/5465/>
- [8] J.-C. Antona, A. Carbo-Meseguer, V. Letellier, ‘‘Evolution of High Capacity Submarine Open Cables,’’ in *Proc. Asia Commun. and Photon. Conf. (APC)*, Chengdu (China), 2019, paper S4B.2.
- [9] C. R. Giles and E. Desurvire, ‘‘Propagation of Signal and Noise in Concatenated Erbium-Doped Fiber Optical Amplifiers,’’ *J. Lightw. Technol.*, vol. 9, no. 2, pp. 147-154, Feb. 1991.
- [10] A. Ghazisaeidi, ‘‘A Theory of Nonlinear Interactions between Signal and Amplified Spontaneous Emission Noise in Coherent Wavelength Division Multiplexed Systems,’’ *J. Lightw. Technol.*, vol. 35, pp. 5150–5175, Dec. 2017.
- [11] A. Splett, C. Kurtzke, and K. Petermann, ‘‘Ultimate transmission capacity of amplified optical fiber communication systems taking into account fiber nonlinearities,’’ in *Proc. European Conf. on Optical Commun. (ECOC)*, Montreux (Switzerland), 1993, paper MoC2.4.
- [12] G. Bosco *et al.*, ‘‘Performance prediction for WDM PM-QPSK transmission over uncompensated links,’’ in *Proc. Opt. Fiber Commun. (OFC)*, San Diego (CA), 2011, paper OThO7.
- [13] E. Grellier and A. Bononi, ‘‘Quality parameter for coherent transmissions with Gaussian-distributed nonlinear noise,’’ *Opt. Exp.*, vol. 19, no. 13, pp. 12781--12788, Jun. 2011.
- [14] A. Carena, *et al.*, ‘‘Modeling of the Impact of Non-Linear Propagation Effects in Uncompensated Optical Coherent Transmission Links,’’ *J. Lightw. Technol.*, vol. 30, no. 10, pp. 1524-1539, may 2012.

- [15] P. Poggiolini, "The GN model of non-linear propagation in uncompensated coherent optical systems," *J. Lightw. Technol.*, vol. 30, no. 24, pp. 3857–3879, Dec. 2012.
- [16] A. Carena *et al.* "EGN model of non-linear fiber propagation," *Opt. Exp.*, vol. 22, no. 13, pp. 16335–16362, Jun. 2014.
- [17] P. Poggiolini *et al.*, "A Simple and Effective Closed-Form GN Model Correction Formula Accounting for Signal Non-Gaussian Distribution," *J. Lightw. Technol.*, vol. 33, no. 2, pp. 459–473, Jan. 2015.
- [18] R. Dar, M. Feder, A. Mecozzi, and M. Shtaif, "Accumulation of nonlinear interference noise in fiber-optic systems," *Opt. Exp.*, vol. 22, no. 12, pp. 14199–14211, Jun. 2014.
- [19] P. Serena, and A. Bononi, "A Time-Domain Extended Gaussian Noise Model," *J. Lightw. Technol.*, vol. 33, no. 7, pp. 1459–1472, Apr. 2015.
- [20] A. Bononi, J.-C. Antona, A. Carbo Méseguer, P. Serena, "A model for the generalized droop formula," in Proc. *European Conf. on Optical Commun. (ECOC)*, Dublin, Ireland, 2019, paper W.1.D.5. Also available with typos corrections at arXiv:1906.08645.
- [21] A. Vannucci, P. Serena, and A. Bononi, "The RP method: a new tool for the iterative solution of the nonlinear Schroedinger equation," *J. Lightw. Technol.*, vol. 20, pp. 1102–1112, Jul. 2002.
- [22] M. Secondini, D. Marsella, and E. Forestieri, "Enhanced split-step Fourier method for digital backpropagation," in Proc. *European Conf. on Optical Commun. (ECOC)*, Cannes, France, 2014, paper We.3.3.5.
- [23] X. Liang and S. Kumar, "Multistage perturbation theory for compensating intra-channel impairments in fiber optic systems," *Opt. Exp.*, vol. 22, no. 24, pp. 29733–29745, Dec. 2014.
- [24] P. Poggiolini, G. Bosco, A. Carena, V. Curri, F. Forghieri, "A Detailed Analytical Derivation of the GN Model of Non-Linear Interference in Coherent Optical Transmission Systems," Available: arXiv:1209.0394, [physics.optics] (2012).
- [25] P. Johannisson and M. Karlsson, "Perturbation analysis of nonlinear propagation in a strongly dispersive optical communication system," *J. Lightw. Technol.* vol. 31, pp. 1273–1282 (2013).
- [26] A. Bononi and P. Serena, "An alternative derivation of Johannisson's regular perturbation model," Available: arXiv:1207.4729, [physics.optics] (2012).
- [27] P. Poggiolini, A. Carena, Y. Jiang, G. Bosco, V. Curri, and F. Forghieri, "Impact of low-OSNR operation on the performance of advanced coherent optical transmission systems," in Proc. *European Conf. on Optical Commun. (ECOC)*, Cannes, France, 2014, paper Mo.4.3.2.
- [28] P. Serena, "Nonlinear Signal–Noise Interaction in Optical Links With Nonlinear Equalization," *J. Lightw. Technol.*, vol. 34, no. 6, pp. 1476–1483, Mar. 2016.
- [29] G. Bosco, V. Curri, A. Carena, P. Poggolini, and F. Forghieri, "On the Performance of Nyquist-WDM Terabit Superchannels Based on PM-BPSK, PM-QPSK, PM-8QAM or PM-16QAM Subcarriers," *J. Lightw. Technol.*, vol. 29, n. 1, pp. 53–61 (2011).
- [30] H. A. Haus, "The Noise Figure of Optical Amplifiers," *Photon. Technol. Lett.*, vol. 10, no. 11, pp. 1602–1604, Nov. 1998.
- [31] F. Vacondio *et al.*, "On nonlinear distortions of highly dispersive optical coherent systems," *Opt. Exp.*, vol. 20, no. 2, pp. 1022–1032, Jan. 2012.
- [32] M. A. Bolshtyansky *et al.*, "Impact of Spontaneous Guided Acoustic-Wave Brillouin Scattering on Long-haul Transmission," in Proc. *Opt. Fiber Commun. (OFC)*, San Diego (CA), 2018, paper M4B.3.
- [33] J. M. Gené and P. J. Winzer "A Universal Specification for Multicore Fiber Crosstalk," *Photon. Technol. Lett.*, vol 31, n. 9, pp. 673–676 (2019).
- [34] H. Louchet, A. Hodzic and K. Petermann, "Analytical model for the performance evaluation of DWDM transmission systems," *Photon. Technol. Lett.*, vol. 15, no. 9, pp. 1219–1221, 2003.